Soil Dynamics and Earthquake Engineering 85 (2016) 202–216

Contents lists available at ScienceDirect

Soil Dynamics and Earthquake Engineering

journal homepage: www.elsevier.com/locate/soildyn

Seismic response of underground reservoir structures in sand: Evaluation of Class-C and C1 numerical simulations using centrifuge experiments

Y.H. Deng [a], S. Dashti [b,*], A. Hushmand [b], C. Davis [c], B. Hushmand [d]

[a] Chang'an University, Department of Geological Engineering, Xi'an, China
[b] University of Colorado Boulder, Civil, Environmental and Architectural Engineering, Boulder, CO, United States
[c] Los Angeles Department of Water and Power, Los Angeles, CA, United States
[d] Hushmand Associates, Inc., Irvine, CA, United States

ARTICLE INFO

Article history:
Received 10 December 2015
Received in revised form
29 March 2016
Accepted 6 April 2016

Keywords:
Centrifuge
Seismic soil-structure interaction
Nonlinear finite element analyses
Buried reservoir structures

ABSTRACT

Centrifuge experiments were conducted to investigate the seismic response of *stiff-unyielding* buried reservoir structures with varying stiffness in medium-dense, dry sand. The results of these tests were used to evaluate the predictive capabilities of Class-C and C1, nonlinear, finite element analyses of the seismic response of these relatively stiff buried structures. All simulations were performed in two dimensions using the pressure-dependent, multi-yield-surface, plasticity-based soil constitutive model (PDMY02) implemented in OpenSees. For Class-C simulations, model parameters were calibrated based on the available cyclic simple shear tests on the test soil. For Class-C1 simulations, the same soil model was used along with user-defined modulus reduction curves that were corrected for soil's implied shear strength. The use of shear modulus reduction curves, which modeled a softer soil response compared to PDMY02, generally improved the prediction of site response in the far-field as well as seismic racking deformations, earth pressures, and bending strains on the structures. Experimentally, the dynamic thrust, racking, and bending strains on or of the model structures were shown to primarily peak near the strain-dependent fundamental frequency of the site, regardless of the fundamental frequency of the structure itself. This influence in addition to other important response parameters were captured reasonably well by Class-C1 simulations, with residuals ranging from −0.25 to 0.2.

1. Introduction

Underground box structures have generally performed well during previous earthquakes except for a few cases of damage (e.g., Daikai Subway Station during the 1995 Hyogo Ken Nanbu Earthquake; Balboa water treatment plant during the 1971 San Fernando Earthquake), which show the importance of designing them safely for seismic loading. The current state of practice for analyzing the seismic performance of underground reservoir structures relies heavily on simplified analytical methods that do not fully capture the kinematic constraints imposed on these structures. These procedures are often either based on the assumption of a *yielding* wall, which displaces sufficiently to develop an active condition (e.g., [19,21,25]), or a *rigid-unyielding* wall, which undergoes no deformation (e.g., [32]). Underground reservoir structures fall in neither of these two extreme categories. They exhibit some deformation depending on their stiffness, but they deform less than a vertical structure buried in the ground. This is because the walls of a reservoir structure are restrained against large deformations at their roof and base [12].

Soil-structure interaction (SSI) near relatively stiff buried structures depends on the stiffness and geometric constraints of the structure, properties of the backfill soil, soil-structure interface properties, and characteristics of the earthquake motion. Advanced numerical tools can model the stiffness and geometric constraints of structures, soil nonlinearities during strong dynamic loading, and the interface conditions between the soil and structure, in order to predict the seismic performance of structures. Previous numerical simulations of the seismic response of yielding or unyielding walls typically used linear, equivalent-linear viscoelastic, or elastic perfectly-plastic backfill soil properties (e.g., [23,24,30,31,36]) to evaluate the influence of wall flexural rigidity, base and translational flexibility, and soil properties on the amplitude and distribution of earth pressures and deformations. Seismic earth pressures on *stiff-unyielding* structures have not been studied adequately using advanced numerical analyses with

* Corresponding author.
E-mail address: shideh.dashti@colorado.edu (S. Dashti).

http://dx.doi.org/10.1016/j.soildyn.2016.04.003
0267-7261/

Table 1
Dimensions and properties of three equivalent model structures used in centrifuge in prototype scale [12].

Structure	Height and width (m) (outer edge to outer edge)	Thickness (cm)			Lateral stiffness (kN/m^2)	Fundamental frequency (Hz)
		Base	Roof	Walls		
Baseline	10.4 and 12.2	69	37	56	9.0	4.0
Flexible		50	28	28	1.8	2.0
Stiff		146	112	113	131.4	9.9

Note: Model structures were 17.46 m long (approximately equal to the inside width of the centrifuge container).

nonlinear, pressure-dependent soil properties and realistic interface conditions. Capturing soil's nonlinear response is particularly important in the analysis of reservoir structures, because they are often designed for strong levels of shaking inducing large strains in the backfill soil. Further, many of the previous numerical methods with realistic conditions were not sufficiently validated against case histories or experimental studies for *stiff-unyielding* structures.

Most of the previous experimental studies have focused on the seismic response of yielding retaining walls [1,5,18,20,22,27,28]. Recent dynamic centrifuge tests have also been performed on relatively flexible, rectangular tunnels in cohesionless soils (e.g., [6,30]). These tunnels, however, were more flexible and buried deeper than those representative of reservoir structures near the surface.

A series of three centrifuge experiments were recently conducted by Hushmand et al. [12] at the University of Colorado Boulder to evaluate the seismic performance of relatively stiff underground structures buried in an 18.6 m-thick layer of dry, Nevada Sand at a relative density (D_r) of approximately 60%. Three different model box structures were designed to represent simplified prototype reinforced concrete buried reservoir structures of varying stiffness characterizing those evaluated by the Los Angeles Department of Water and Power (LADWP). The structures had 10.4 m high walls that were restrained against rotational movement at the top and bottom by their roof and floor. Additionally, the reservoir's foundation could rock or slide on the soil. Hushmand et al. [12] showed experimentally that none of the commonly used procedures (e.g., [2,19,21,25,32]) could adequately capture the loading and deformations experienced by reservoir structures for the range of stiffness and ground motions considered in their design. These experiments enabled a comprehensive and fundamental evaluation of the influence of structure stiffness and ground motion characteristics on seismic SSI as well as lateral earth pressures, racking deformations, and bending strains experienced by *stiff-unyielding* buried structures.

The centrifuge experiments performed by Hushmand et al. [12] are used in this paper to evaluate the ability of Class-C and C1, nonlinear finite element analyses of the soil-structure system in simulating the response of *stiff-unyielding* structures buried in medium-dense, dry sand. Even though centrifuge experiments do not represent the complexities of real field conditions, they enable validation of numerical tools that may later be used in modeling more complex conditions. The prediction classification used in this paper is based on that described by Lambe [16]. A Class-C prediction is one made after the experiment without knowing the results at the time of the prediction. A Class-C1 prediction is one made after the event, while knowing the results of the experiment at the time of prediction.

All simulations of the centrifuge tests presented in this paper were performed using the pressure-dependent, multi-yield-surface, plasticity-based soil constitutive model (PDMY02) implemented in OpenSees by Elgamal et al. [9] and Yang et al. [34,35]. The PDMY02 soil constitutive model parameters for Class-C simulations were calibrated based on the available cyclic simple shear tests (e.g., detailed by Karimi and Dashti [14,15]) on the test soil. Class-C1 simulations were performed with the same soil model as the Class-C but with manually adjusted shear modulus reduction curves, in order to better capture centrifuge experimental results. In this paper, we discuss and compare the predictive ability of Class-C and C1, nonlinear finite element simulations in capturing seismic SSI, accelerations, deformations, and lateral earth pressures on underground reservoir structures.

2. Overview of centrifugre experiments

A series of three centrifuge experiments were conducted at the University of Colorado Boulder, all with similar soil conditions, instrumentation, and structure outer dimensions but different thickness and stiffness of the model underground structures. These three tests, referred to as T-Flexible, T-Baseline (or T-BL), and T-Stiff, were named according to the relative stiffness of the underground structure, as detailed by Hushmand et al. [12]. All the three models were spun to 60 g of centrifugal acceleration, and a sequence of five earthquake motions were applied to the model specimen in flight in the same order. All the dimensions presented in this paper are in prototype scale, unless stated otherwise.

2.1. Properties of underground structures

Three simplified, equivalent, scaled box structures were designed in centrifuge to simulate the mass, lateral stiffness, and natural frequency of complex prototype, buried, reinforced concrete, water reservoir structures. The structures were designed with uniform 1018 Carbon Steel (density = 7870 kg/m^3; Young's Modulus = 200 GPa; Poisson's ratio = 0.29). As summarized in Table 1, the outer dimensions of the three structures were kept the same, while their thicknesses were varied to change their stiffness.

2.2. Soil properties, model preparation, and instrumentation

Fig. 1 shows the model configuration and instrumentation in the three experiments. Nevada sand ($G_s = 2.65$; $e_{min} = 0.56$; $e_{max} = 0.84$; $D_{50} = 0.13$ mm; $C_u = 1.67$) was dry pluviated into a flexible-shear-beam (FSB) centrifuge container to achieve a uniform soil layer with a relative density of $D_r \approx 60\%$ or a dry unit weight of 15.6 kN/m^3. The transfer functions of surface to base accelerations in the far-field under centrifuge ambient vibrations indicated a small-strain, soil fundamental frequency (f_{so}) ranging from about 2.1 to 2.4 Hz (corresponding to an average, small-strain, shear wave velocity, $\bar{V}s$, ranging from about 156 to 179 m/s), while the transfer functions obtained from earthquake motions indicated strain-dependent, effective site fundamental frequencies (f_{so}') ranging from about 1.0 to 1.7 Hz (average, effective $\bar{V}s$' ranging from 74 to 126 m/s). The estimated small strain $\bar{V}s$ of the far-field soil prior to shaking agreed with but was slightly smaller than those estimated using the empirical procedures recommended by Seed and Idriss [26] and Bardet et al. [4] for sand.

Teflon sheets were used on the container sides and ends of the structures to reduce friction at the structure-container interface.

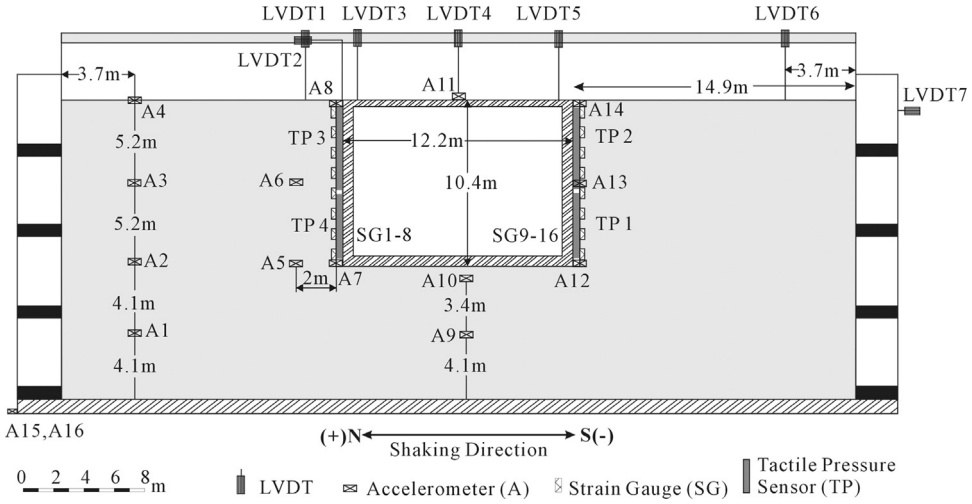

Fig. 1. Schematic and layout of centrifuge experiments in prototype scale [12].

Nevada sand was glued to the base of the structures to provide a more realistic interface friction between the structure and the soil. As shown in Fig. 1, data was collected with accelerometers, tactile pressure sensors, strain gauges, and LVDTs. The accelerometer array A1-4 representing far-field conditions (approximating free-field) was placed 11.1 m from the wall of the structure and 3.7 m from the inner boundary of the flexible container. Even though use of an FSB container is expected to reduce boundary effects, the far-field location in these experiments was likely still influenced to some degree by boundary effects as well as soil-structure interaction. Therefore, it was important to mimic similar conditions numerically for a proper comparison, as opposed to simulating a true free-field condition. The tactile sensors were first thoroughly de-aired, conditioned, equilibrated, and calibrated statically according to the procedure recommended by Tessari et al. [29]. Then, they were dynamically calibrated using the procedure described by Gillis et al. [10].

2.3. Ground motions

Scaled, horizontal components of the following recordings were applied to the base of the model in each experiment: Sylmar Converter Station during the 1994 Northridge Earthquake (NSC52), the LGPC Station during the 1989 Loma Prieta Earthquake (LGP000), and the Istanbul Station during the 1999 Izmit Earthquake in Turkey (IST180). These motions were chosen to evaluate the influence of different ground motion characteristics (i.e., in terms of intensity, frequency content, and duration) on the performance of the buried structures and their interaction with the surrounding soil. Fig. 2 shows the acceleration response spectra (5% damped) and Arias Intensity time histories of the base motions achieved (or measured) in T-BL, and Hushmand et al. [12] provided more details on their properties. The achieved base motions varied slightly during different experiments because of the variation in model weights and natural frequencies. Therefore, it was important to use the actual recording of the base motion during the numerical simulation of the corresponding test.

3. Numerical simulations

The centrifuge tests described in the previous section were numerically simulated using the pressure-dependent, multi-yield-surface, plasticity-based soil model (PDMY02) implemented in OpenSees by Elgamal et al. [9] and Yang et al. [34]. Nonlinear soil constitutive models have many parameters to calibrate, often making them impractical in engineering design. However, in the seismic design of underground reservoir structures, strong ground motions are regularly selected due to the sensitivity of these structures. Under such strong levels of shaking and shear strains, equivalent-linear viscoelastic or elastic perfectly-plastic soil constitutive models become increasingly limiting. Hence, the PDMY02 model, despite its many parameters, was used in this study to model the nonlinear behavior of the retained soil. Hashash et al.

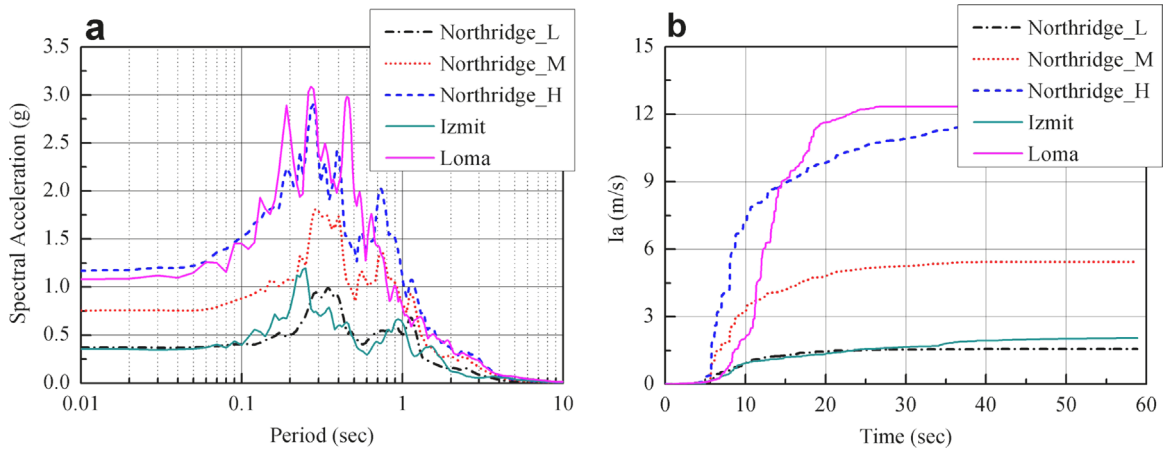

Fig. 2. Container base motions as recorded in T-BL and input into the numerical simulations: (a) 5%-damped spectral accelerations; and (b) Arias Intensity time histories.

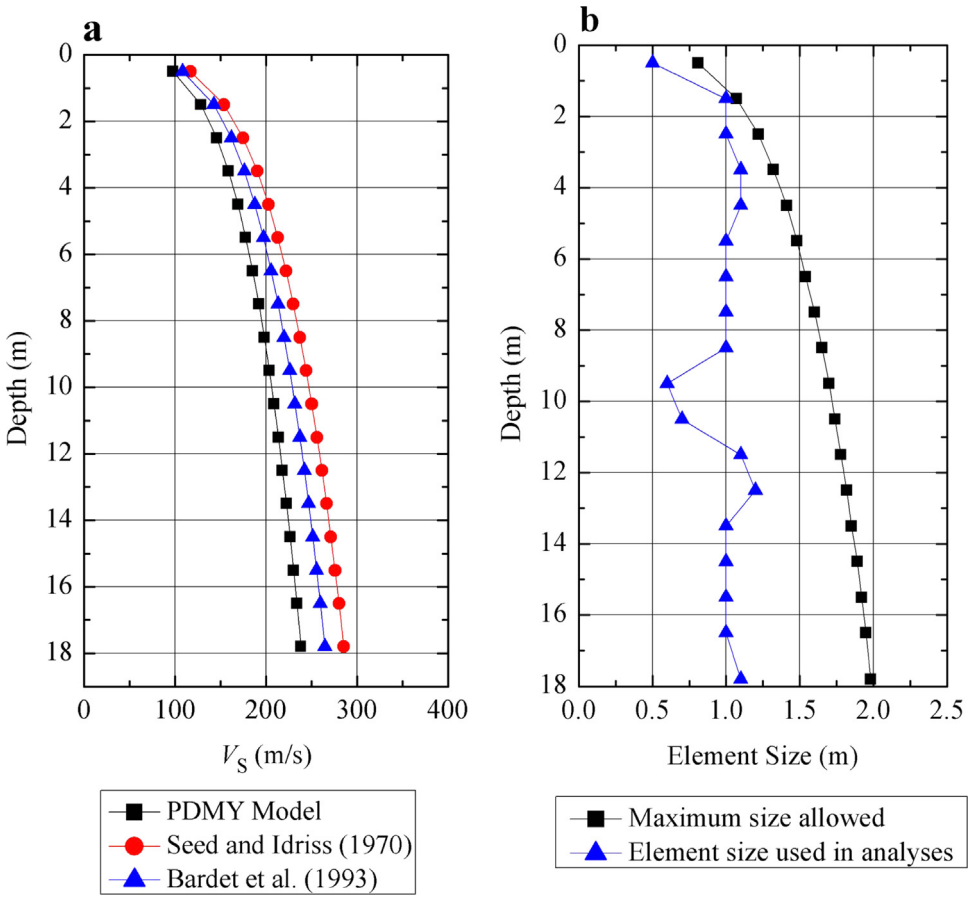

Fig. 3. (a) The small-strain V_s profile used in the numerical simulations of Nevada sand compared with two empirical procedures; (b) the maximum allowed and selected element size with depth.

[11] showed the promise of this constitutive model in analyzing site response in medium-dense, dry sand as compared to centrifuge measurements, when combined with user-defined modulus reduction curves expected for the test soil. The numerical analyses presented in this paper were conducted in prototype scale and in two dimensions (2-D) assuming plane strain conditions.

Soil and underground structures were all modeled using SSPquad elements [17]. A linear-elastic material was adopted to simulate the response of the underground structures, with appropriate properties (density, Young's modulus, and Poisson's ratio). Node-to-segment, frictional contact, zero-length interface elements of type zeroLengthContactNTS2D [33] were used between soil and structure elements to allow for relative movements between the soil and a buried structure. This interface element follows the classical Coulomb friction law, and the interface friction was defined as $\tan(\phi_{interface})=0.7\ \tan(\phi_{soil})$.

The element size was selected to allow shear wave propagation in the frequency range of interest. Fig. 3a shows the small-strain V_s profile in soil predicted from two empirical equations compared to the default estimates by the PDMY02 model. A maximum frequency (f_{max}) of 15 Hz was conservatively assumed during dynamic loading, which was beyond the capacity of the shaking table under increased gravity (typically around 400 Hz in model scale, which translates to 6.7 Hz in prototype scale). The maximum allowable element size at each depth was then estimated as: $h_{allowable}$=minimum wavelength/8=$\lambda_{min}/8=(V_s/f_{max})/8$. The adopted mesh size was smaller than the maximum allowable size, as shown in Fig. 3b. Fig. 4 shows the mesh configuration of a

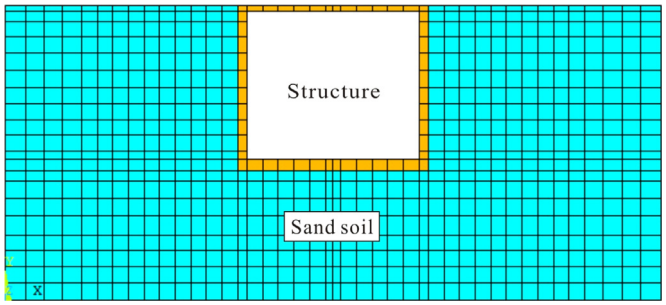

Fig. 4. The mesh configuration used in the numerical simulation of centrifuge experiments.

representative model (T-BL). The displacement degrees of freedom were tied for each pair of nodes on side boundaries at the same elevation, to represent the physical conditions imposed by the centrifuge container.

The PDMY02 soil constitutive model parameters for Class-C simulations were calibrated based on the available cyclic simple shear (CSS) tests on Nevada sand with different values of confining stress, relative density, and cyclic stress ratio performed by Arulmoli et al. [3] and Kammerer et al. [13]. Karimi and Dashti [14,15] provided a comparison of the numerically simulated (using the PDMY02 model) and experimentally measured soil response at an element level in CSS tests, which are not repeated here for brevity. Table 2 summarizes the calibrated soil model parameters used in this study.

The same motions recorded in each centrifuge test were applied to the base of the corresponding numerical model in the

Table 2
Summary of PDMY model parameters for Nevada sand [14,15].

Parameter	Value					Unit	Description
D_r	60	61	64	69	74	%	Relative density
e	0.67	0.67	0.66	0.65	0.64	–	Void ratio
ρ	1.59	1.59	1.60	1.61	1.62	ton/m^3	Saturated unit weight
p_r'	101	101	101	101	101	kPa	Reference effective confining pressure
$G_{max,1,oct}$	68.95	70.25	73.42	78.23	83.86	MPa	Octahedral low-strain shear modulus
$\gamma_{max,r}$	0.1	0.1	0.1	0.1	0.1	–	Maximum octahedral shear strain
B_r	184.09	187.57	196.06	208.91	223.95	MPa	Bulk modulus
d	0.5	0.5	0.5	0.5	0.5	–	Pressure dependency coefficient
φ_{TXC}	34.3	34.3	34.8	36.2	37.1	deg.	Triaxial friction angle used by model
φ_{PT}	26.3	26.3	26.4	26.0	26.1	deg.	Phase transformation angle
c_1	0.040	0.042	0.036	0.020	0.019	–	Control the shear-induced volumetric change, contraction tendency based on the dilation history, and
c_2	2.85	2.72	2.30	1.50	1.49	–	overburden stress effect, respectively
c_3	0.21	0.21	0.19	0.15	0.15	–	
d_1	0.07	0.07	0.09	0.15	0.18	–	Reflect dilation tendency, stress history, and overburden stress, respectively
d_2	3.0	3.0	3.0	3.0	3.0	–	
d_3	0.0	0.0	0.0	0.0	0.0	–	
NYS	20	20	20	20	20	–	Number of yield surfaces generated by model
liq_1	1.0	1.0	1.0	1.0	1.0	–	Account for permanent shear strain (slip strain or cyclic mobility) in sloping ground
liq_2	0.0	0.0	0.0	0.0	0.0	–	

same sequence. After the application of each motion, the soil densified, as confirmed by LVDT recordings at different locations. The far-field settlement measurements in each test were used to estimate, in a simplistic manner, the change in soil relative density (D_r) under 1-D conditions. This change in soil D_r was taken into account in estimating soil model parameters for the subsequent motions in the numerical simulations, as shown in Table 2.

No modulus reduction curve was used other than that predicted by default by the PDMY02 model in OpenSees for Class-C predictions. A small-strain, Rayleigh damping value of 2% was implemented at the fundamental frequency of the site. Based on the comparison of Class-C numerical results with experimental measurements, particularly the response in the far-field, Class-C1 simulations were performed with the same soil constitutive model parameters as Class-C but this time with user-defined, shear modulus reduction curves (G/G_{max} versus γ) that were corrected for soil's implied shear strength (similar to the approach taken by [11]), in order to better capture the response measured in centrifuge. Table 3 summarizes the parameters used to obtain the mean and one standard deviation above mean (upper) G/G_{max} curves proposed by Darendeli [7], and Fig. 5 compares these curves with the default response of the PDMY02 model. The reasons behind using these Darendeli's curves in Class-C1 simulations and the comparison of results with centrifuge recordings will be discussed in the following sections.

Table 3
Parameters used to obtain [7] modulus reduction curves for Nevada sand.

Parameters	Values
K_0	0.44
PI (%)	0
N (cycles)	10
f (Hz)	1
OCR	1

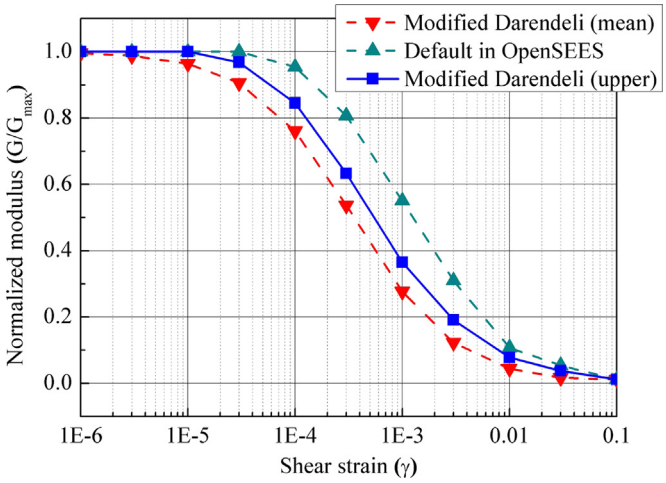

Fig. 5. Normalized modulus reduction curves used in the Class-C and C1 numerical simulations. Class-C simulations used the default PDMY02 curve in OpenSees. Class-C1 simulations used the mean and mean+1 standard deviation (upper) curves proposed by Darendeli [7].

4. Comparison of experimental and numerical results

4.1. Accelerations in the far-field and on the structure

Evaluation of numerical predictions started with site performance (in terms of acceleration and settlement) in the far-field, a location away from the buried structures to minimize the complexities introduced by soil-structure interaction. The goal was to evaluate the ability of nonlinear, time-domain, site-response analyses in capturing the 1-D propagation of horizontal shear waves through uniform dry sand, the strain-compatible effective fundamental frequency (f_{so}') of the site, and shaking-induced permanent settlements in the far-field. The transfer function (TF) of accelerations at the soil surface in the far-field to container base were first compared among the experiments and simulations, as shown in Fig. 6 for a representative experiment (T-BL) and three representative motions. Fig. 7 compares numerically predicted accelerations with those measured in centrifuge along the far-field

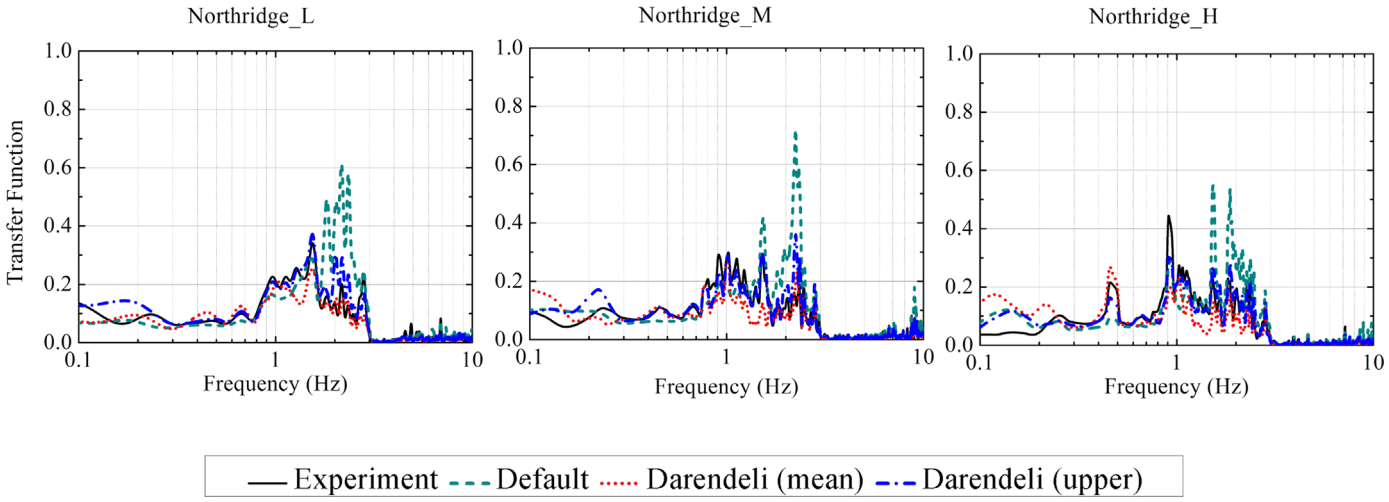

Fig. 6. Experimental and numerical transfer functions (TFs) of surface to base acceleration in the far-field in T-BL during three representative motions.

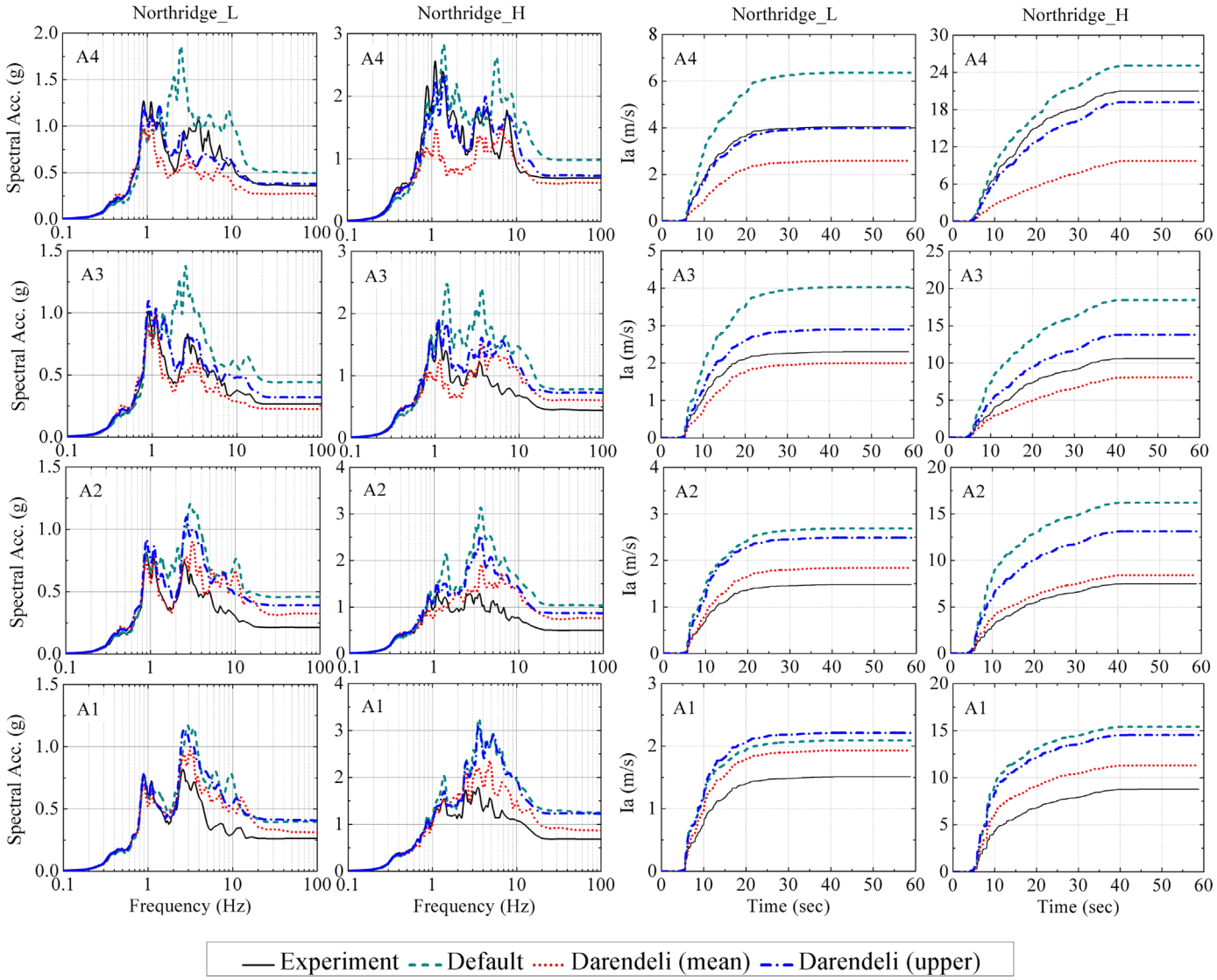

Fig. 7. Experimental and numerical 5%-damped spectral accelerations and Arias Intensity-time histories in the far-field during the Northridge_L and Northridge_H motions in T-BL.

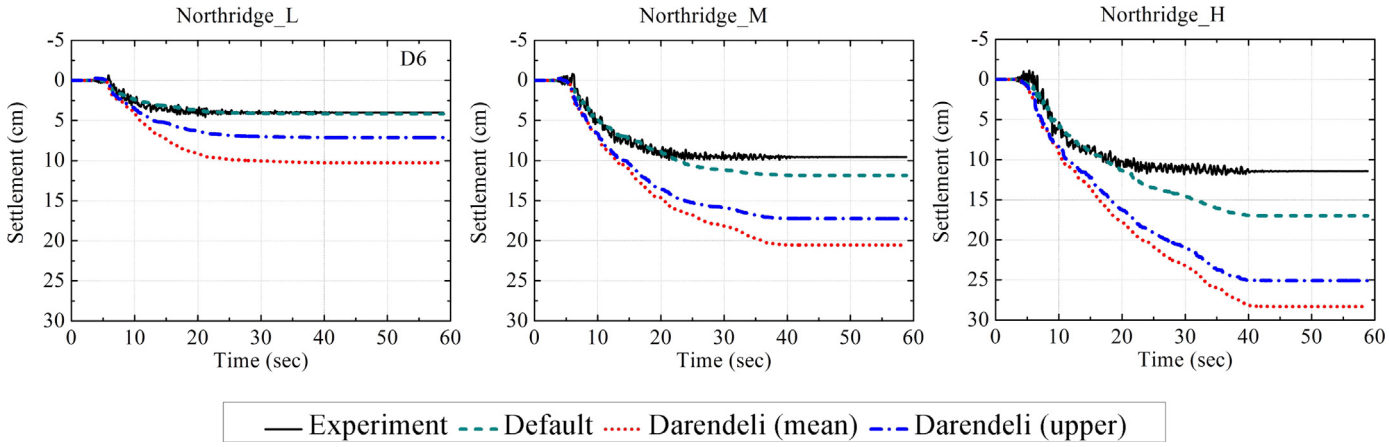

Fig. 8. Experimental and numerical settlements in the far-field during three representative motions in T-BL.

soil column in terms of 5%-damped acceleration response spectra and Arias Intensity time histories. Fig. 8 compares numerically predicted soil surface settlements in the far-field with those measured during different motions.

The f_{so}' of the far-field soil corresponding to the peak value of surface to base TF's was experimentally observed to range from approximately 1–1.7 Hz during the motions employed in this study. Although far-field surface settlements were predicted well

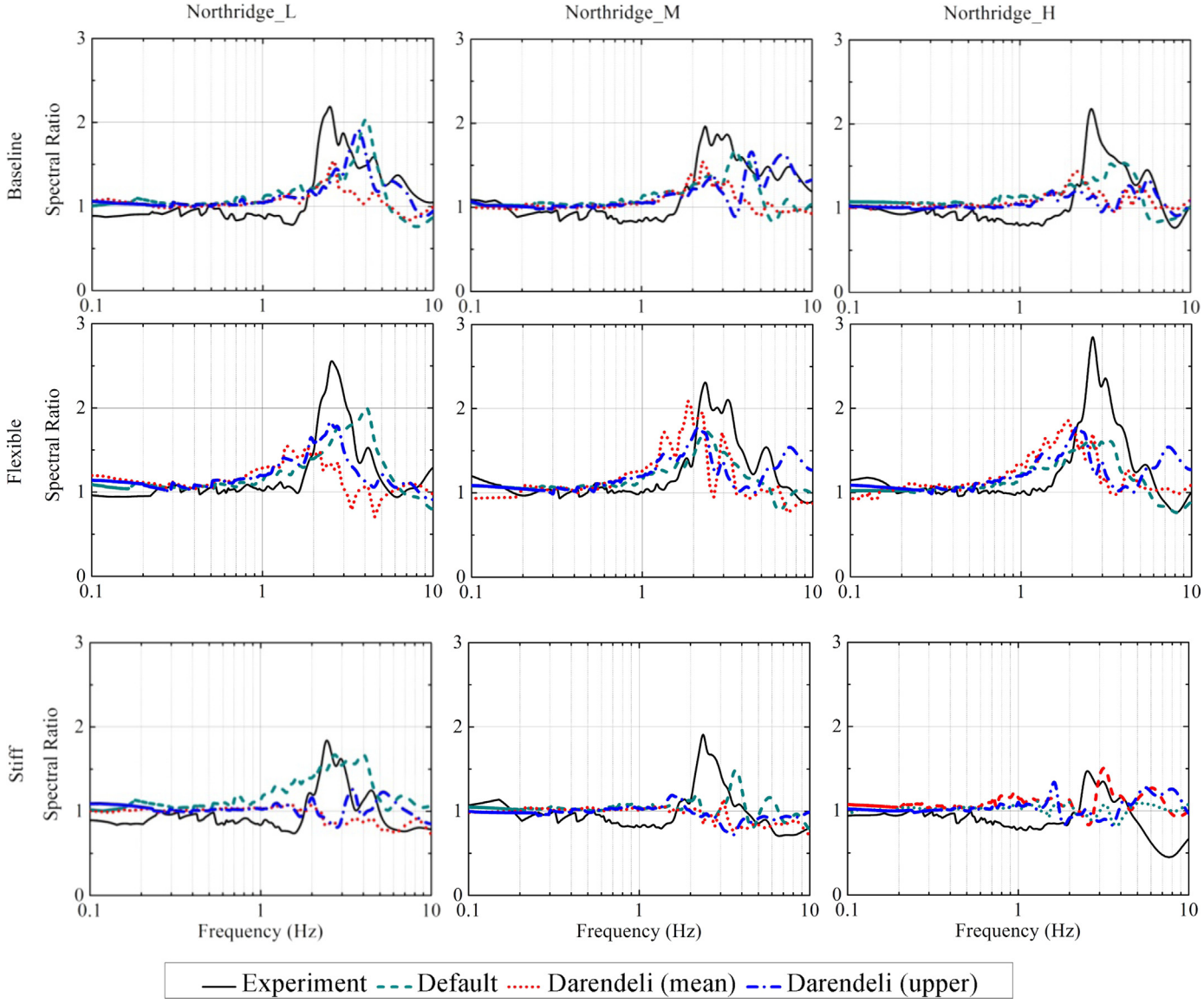

Fig. 9. Experimental and numerical spectral ratios of structure to far-field acceleration (5%-damped) for different structures and three representative ground motions.

by Class-C simulations (Fig. 8), the amplification of accelerations at higher frequencies and hence, the f_{so}' of the site were overestimated during all motions (Fig. 6). This also led to the overestimation of acceleration response spectra at higher frequencies as well as Arias Intensities, particularly near the soil surface in the far-field (Fig. 7). In Class-C predictions, the shear modulus reduction of soil was estimated automatically by the PDMY02 model (Fig. 5). From the far-field comparisons, the soil behavior predicted by the PDMY02 model was judged to be too stiff.

The effective fundamental frequency of the site (f_{so}') was known to have a significant impact on the response of relatively stiff underground reservoir structures, as demonstrated experimentally by Hushmand et al. [12]. Therefore, in Class-C1 predictions, slightly reduced G/G_{max} curves (the mean and mean+1 standard deviation curves proposed by Darendeli [7]) were manually defined in OpenSees to better match the acceleration response in the far-field. These user-defined curves were corrected for the implied shear strength of soil (e.g., [11]). The predicted accelerations and f_{so}' generally improved near the surface, particularly with the use of the upper (i.e. mean+1 standard deviation) Darendeli G/G_{max} curves, as shown in Figs. 6 and 7. Using a softer soil response in OpenSees, however, increased the error in the predicted far-field settlements, as shown in Fig. 8.

The change in accelerations due to the presence of the underground structure was monitored experimentally and numerically, to evaluate the influence of soil-structure interaction (SSI) on accelerations near buried reservoir structures. Fig. 9 compares the numerically predicted and experimentally measured spectral ratios of acceleration at the roof of the structure to that in the far-field soil surface during three representative motions. Experimentally, increasing the confinement and structure stiffness were observed to reduce the amplification of structure to far-field spectral ratios. This pattern was captured numerically. However, near the roof, all numerical simulations slightly underestimated the amplification of accelerations on the structure. The connection between soil and structure elements were therefore slightly too stiff, restraining the independent horizontal movement of the structure near its roof compared to what was observed experimentally, as shown in Fig. 9. Further, Class-C predictions with the default, stiffer, PDMY02 modulus reduction response often overestimated the frequency at which the peak spectral ratios occurred.

4.2. Racking deformations in the far-field and on the structure and numerical settlements in the far-field

Seismically-induced racking displacement, defined as the relative lateral displacement of the structure's roof with respect to its base, is an important measure of seismic performance for underground box structures. Experimentally, racking deformations were obtained both in the far-field and on the structure from double integrating and subtracting accelerometer recordings at the elevations corresponding to the structure's roof and base [12]. A band-pass, 5th order, acausal, Butterworth filter with corner frequencies of 0.2 and 15 Hz was applied to acceleration records, followed by double integration and baseline correction to obtain displacement from accelerometers A12 and A14 on the structure and A2 and A4 in the far-field. Since the structures were designed to remain elastic, no permanent racking was expected, and therefore using accelerometers was judged to be adequate.

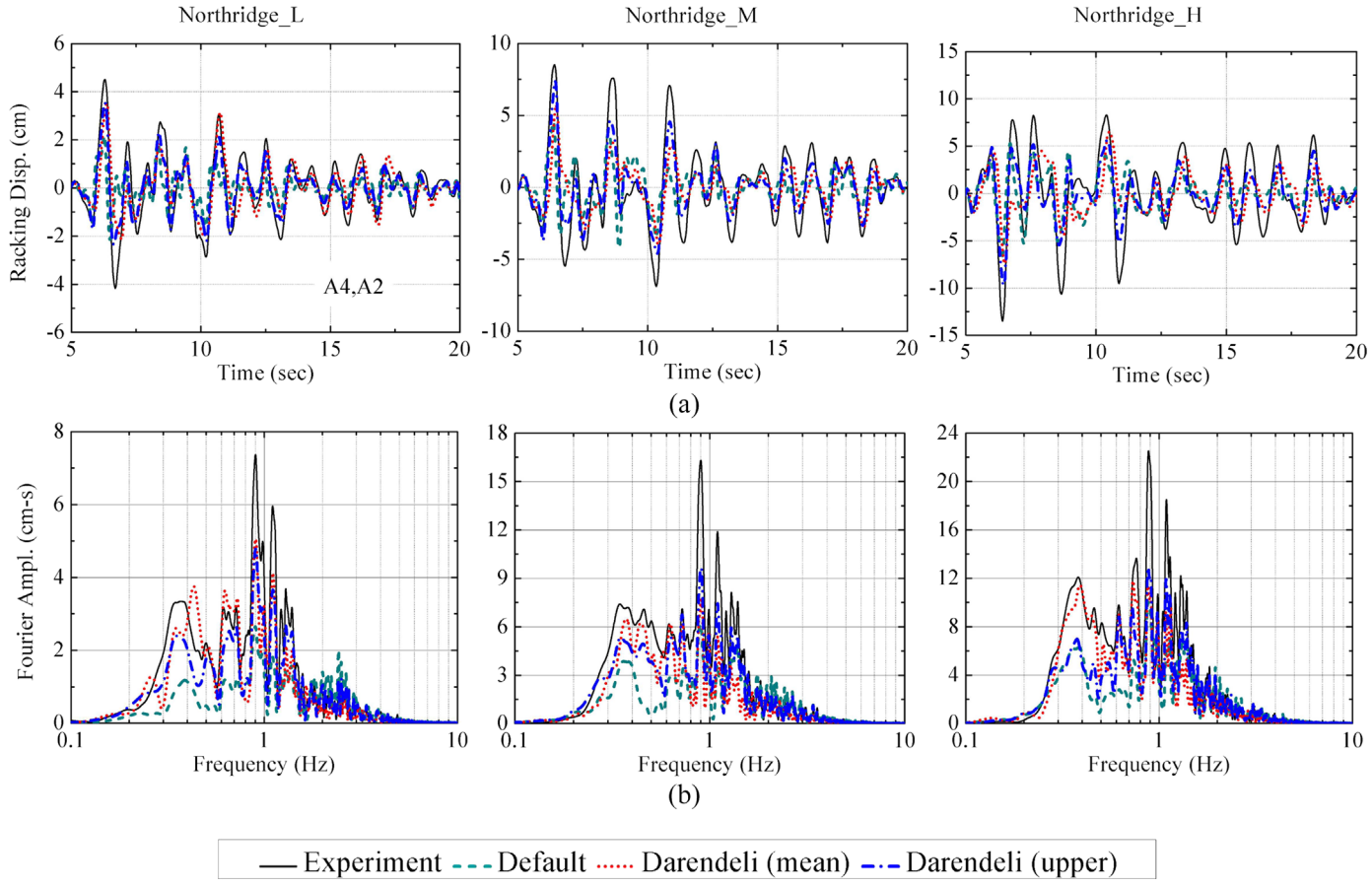

Fig. 10. Experimental recordings and numerical predictions of racking in the far-field during three representative motions in T-BL: (a) time histories zoomed to 5–20 s for clarity; (b) Fourier Amplitude Spectra.

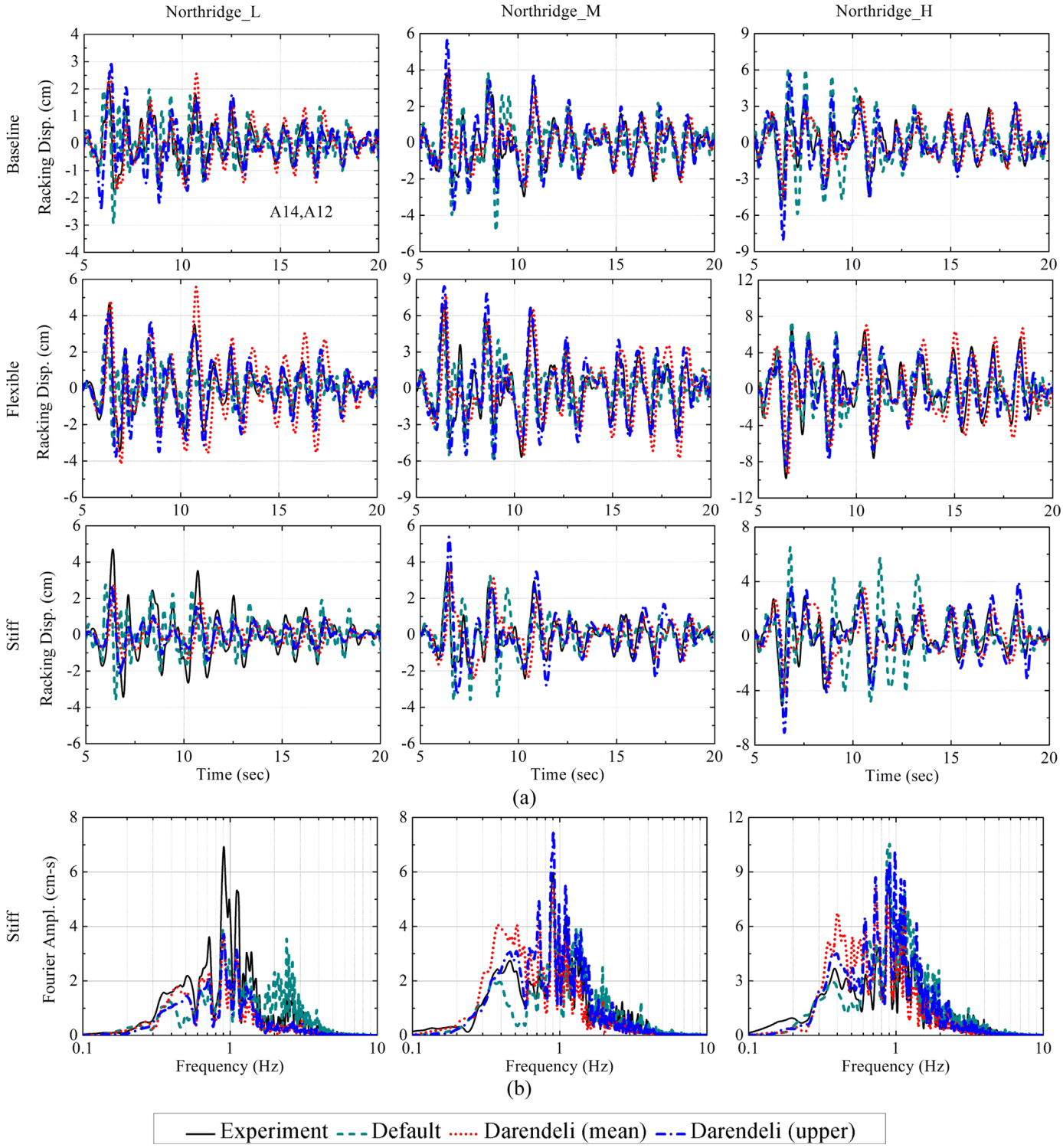

Fig. 11. Experimental recordings and numerical predictions of racking on three different structures during three representative motions in T-BL, T-Flexible, and T-Stiff: (a) time histories zoomed to 5–20 s for clarity; (b) representative Fourier Amplitude Spectra in T-Stiff.

Numerically, racking displacements were obtained directly from the predicted lateral displacements.

Figs. 10 and 11 compare numerically predicted and experimentally recorded seismic racking displacements in the far-field and on three structures, in terms of time histories and Fourier Amplitude Spectra (FAS). Experimentally, racking deformations both in the far-field and on the structures appeared to have a significant content near 1 Hz, which coincided with the effective fundamental frequency of the site (f_{so}') during these motions. Most simulations, particularly Class-C1 predictions, could capture this effect. Class-C simulations with the default PDMY02 model G/G_{max} curve often slightly overestimated racking at higher frequencies and underestimated racking at lower frequencies both in the far-field and on the structures. As expected from the results in terms of far-field accelerations, Class-C1 predictions with the upper Darendeli G/G_{max} curve generally predicted racking better than other simulations, particularly on the structure. Use of the mean Darendeli G/G_{max} curve often led

to an overestimation of structural racking at lower frequencies because of a softer retained soil.

4.3. Lateral earth pressures on the structure

Evaluating the predictive capabilities of nonlinear numerical simulations in terms of seismic lateral earth pressures was one of the main objectives of this study, due to their critical importance in design. To obtain lateral earth pressures experimentally, tactile pressure sensors were employed. These sensors were conditioned, equilibrated, and calibrated both statically and dynamically, as detailed by Gillis et al. [10]. It was shown experimentally that dynamic earth pressures acting on *stiff-unyielding* structures can be of engineering significance and need to be considered in design [12]. Further, the distribution of dynamic earth pressures appeared to change from approximately triangular (increasing with depth) to a higher order polynomial as the flexural rigidity of the wall increased.

Dynamic thrust was obtained experimentally on the structure wall by numerically integrating the dynamic earth pressures along the height of the wall at each instance of time. The dynamic thrust time histories obtained from tactile sensors were subject to a band-pass, 5th order, acausal, Butterworth filter with corner frequencies of 0.1 and 15 Hz, to remove low and high frequency noise that was at times present in the recordings. As a result, any permanent change in thrust could not be captured after filtering. From these time histories, however, the time corresponding to peak thrust could be determined during each ground motion [12]. Dynamic thrust was similarly obtained numerically by integrating dynamic earth pressures along the height of the wall. For a consistent comparison with experimental measurements, a similar

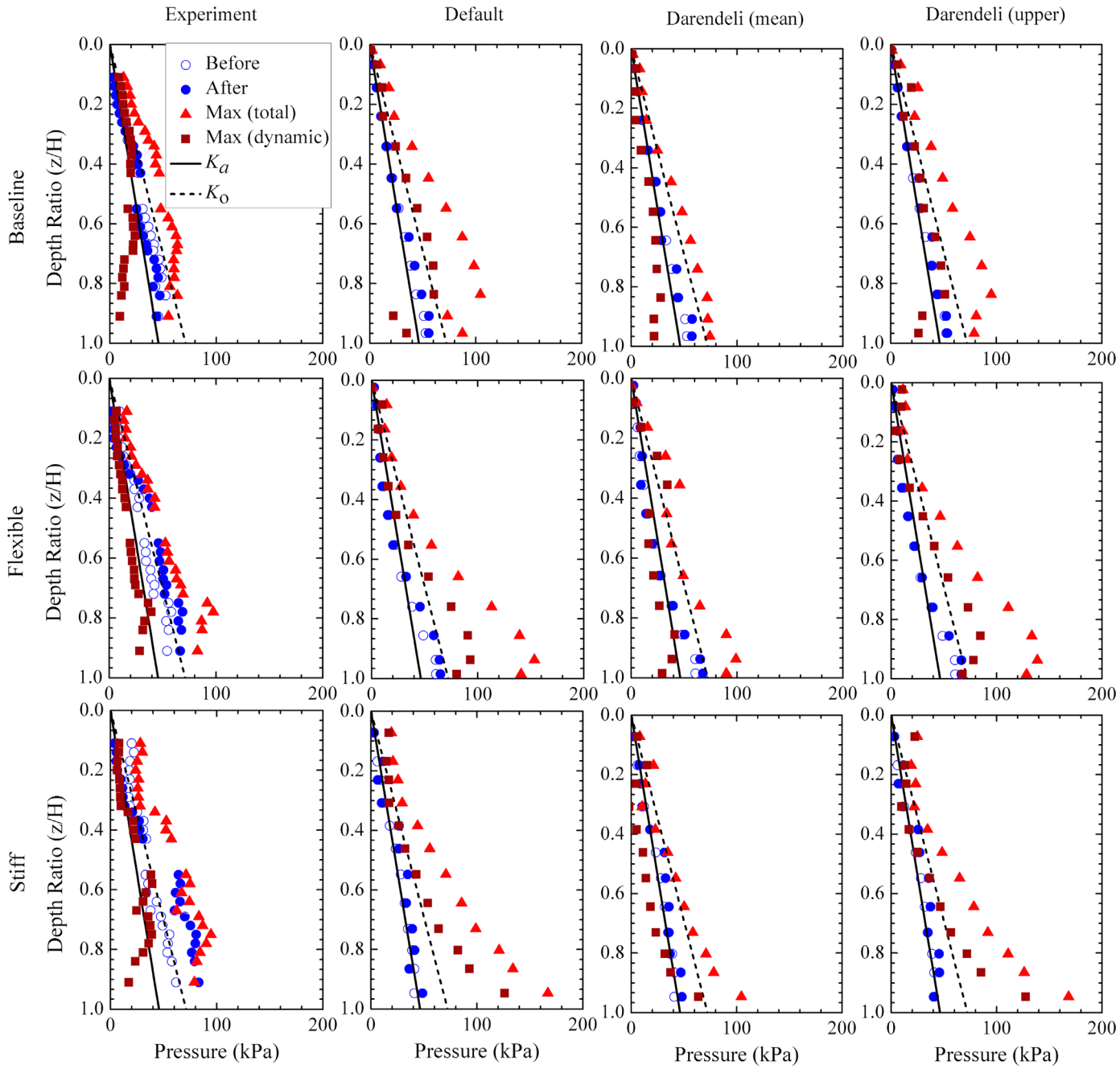

Fig. 12. Static (before and after shaking), total (static+dynamic), and dynamic lateral earth pressure profiles at the time of maximum dynamic thrust on different structures during the Northridge-L motion.

filter was applied to numerically predicted dynamic thrust time histories to remove any permanent change in thrust.

Fig. 12 compares numerically predicted static (before and after the motion prior to filtering), maximum total (static+dynamic), and maximum dynamic lateral earth pressure profiles with those measured in different experiments during the Northridge_L motion. The maximum total and dynamic earth pressures are shown at the time corresponding to peak dynamic thrust in each experiment or simulation. The results are also compared with the theoretically expected static lateral earth pressures under at-rest (K_o) and active (K_a) conditions. All simulations predicted static, pre-shake earth pressures well, which often fell between at-rest and active conditions. The experimentally observed permanent increase in static earth pressures due to earthquake loading was, however, largely underestimated numerically. This is because the numerical model does not update soil properties and changes in soil density and contact of grains with the wall during a time domain analysis.

Total and dynamic earth pressures at the time of peak dynamic thrust were generally overestimated by the stiffer soil models

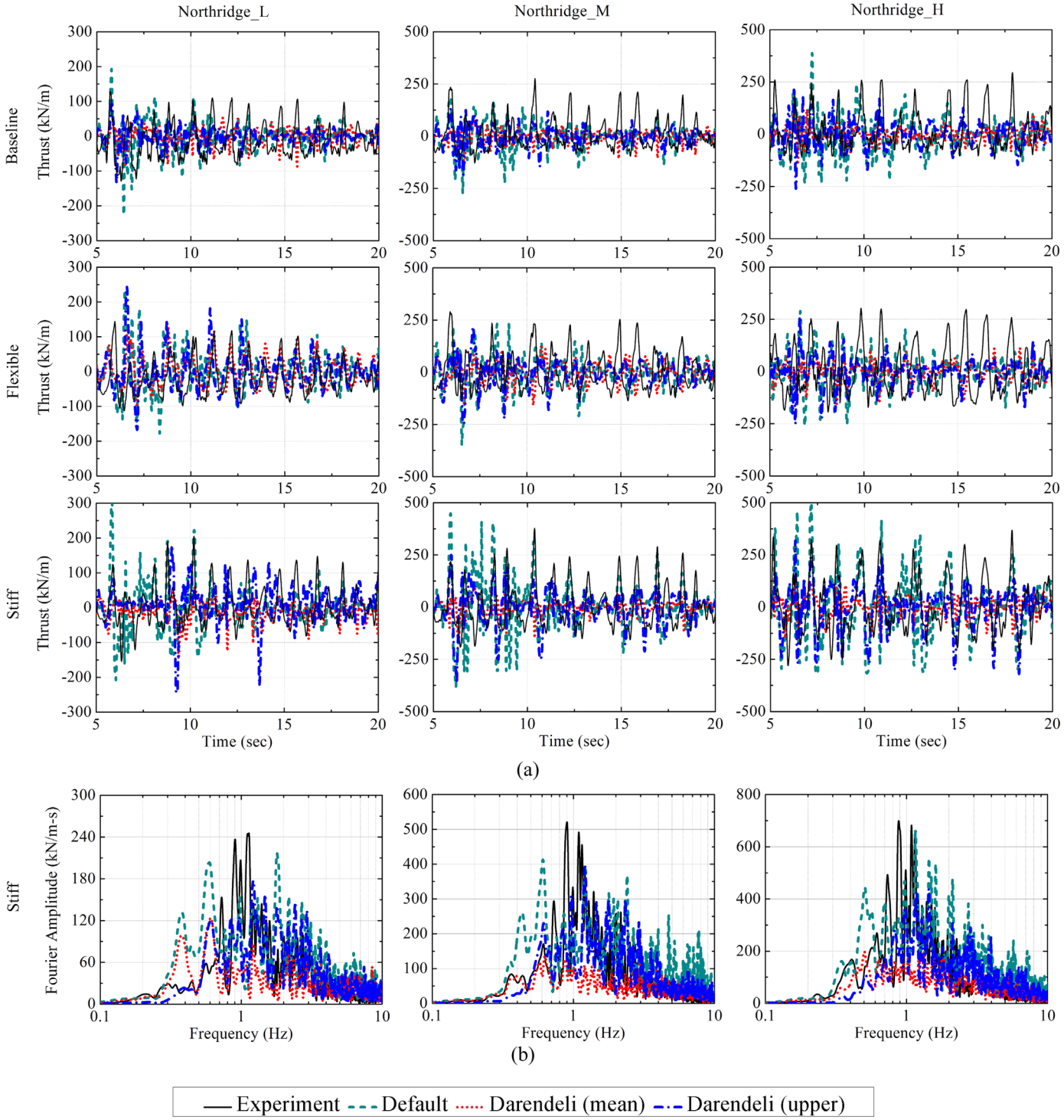

Fig. 13. Experimentally measured and numerically predicted dynamic thrust on different structures during three representative motions: (a) time histories zoomed to 5–20 s for clarify; (b) representative Fourier Amplitude Spectra in T-Stiff.

(default PDMY02 and upper Darendeli) and in some cases slightly underestimated by the softer soil model (mean Darendeli), particularly at shallow depths. The distribution of dynamic earth pressures was better captured by Class-C1 simulations with the mean Darendeli G/G_{max} curve implemented. All simulations, however, failed to predict a parabolic distribution of dynamic earth pressures on the stiff structure and instead predicted a roughly triangular distribution increasing with depth. This was contrary to previous experimental observations.

Friction was minimized on the face of the tactile sensors by using Teflon sheets (as detailed by Gillis et al. [10]) to reduce shear stresses on the sensors and improve their reliability in measuring normal pressure. However, this interface condition is different from what is typically expected on the walls of buried, reinforced concrete, reservoir structures and what was assumed in the numerical simulations. This difference may have been partly responsible for the observed differences in the predicted and measured lateral earth pressures in all Class-C and C1 simulations. In

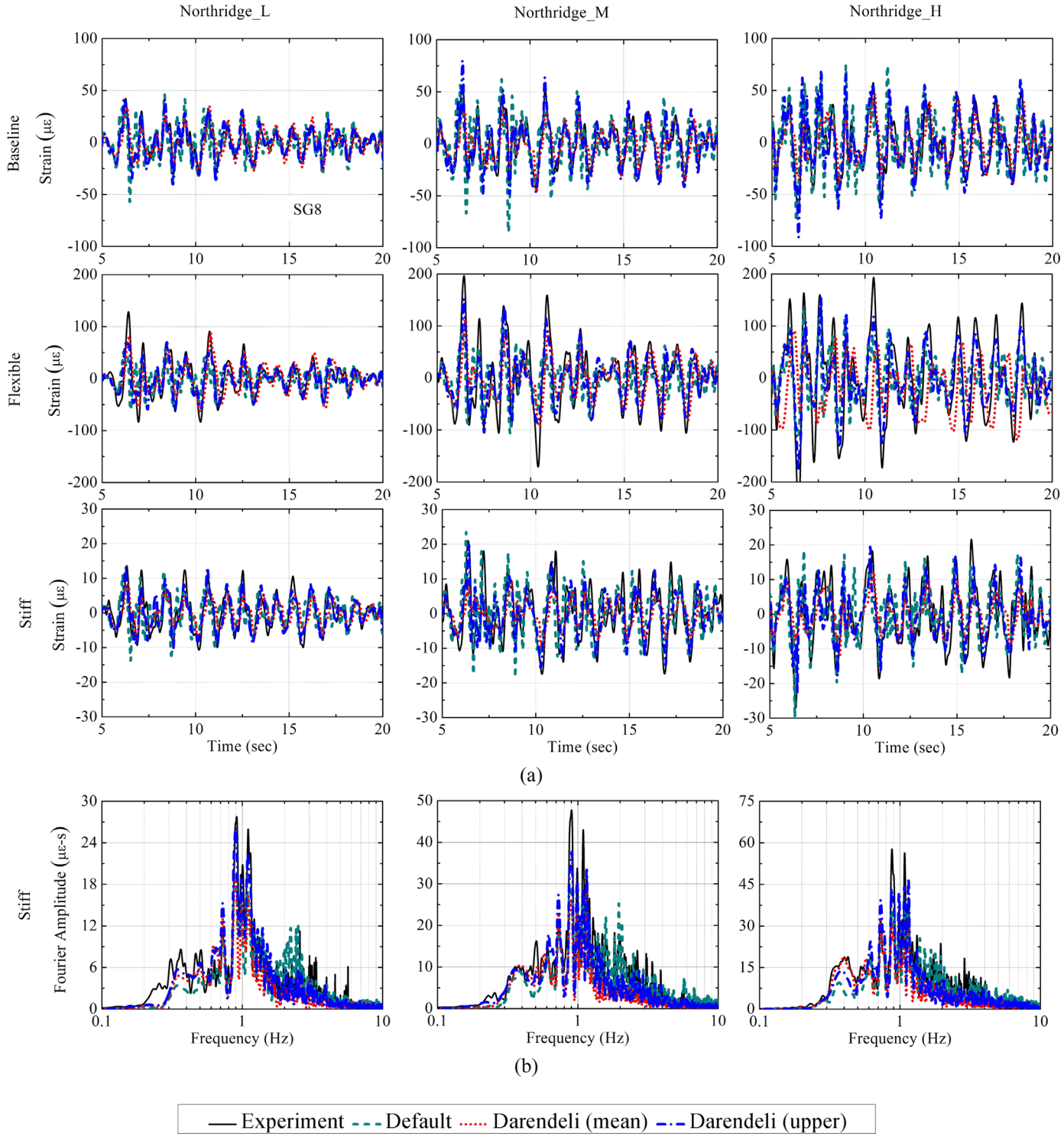

Fig. 14. Experimentally measured and numerically predicted bending strains at the corner of different structures during three representative motions: (a) time histories zoomed to 5–20 s; (b) representative Fourier Amplitude Spectra in T-Stiff.

addition, nonlinear interface properties and complex densification patterns of granular soils around the walls during shaking are difficult to replicate numerically with a continuum model.

Numerically predicted dynamic thrust was compared with those measured in centrifuge for different structures and motions in Fig. 13 in terms of time histories and Fourier Amplitude Spectra, respectively. Experimentally, dynamic thrust on all structures (regardless of its fundamental frequency) always showed significant content near the effective fundamental frequency of the site (f_{so}'), which was approximately 1–1.7 Hz during the motions considered, as shown in Fig. 13b. The stiffer soil model (default PDMY02) often overestimated the peak dynamic thrust and failed to capture the large content near site f_{so}'. Generally, the predictions improved in Class-C1 simulations, particularly with the upper Darendeli curve, although all models tended to underestimate dynamic thrust near the dominant frequencies of 1–1.7 Hz.

4.4. Dynamic bending strains on the structure

The amplitude and distribution of dynamic bending strains were another important measure of the demand imposed on each structure and its performance during earthquake loading. Experimentally, dynamic bending strains were obtained from eight strain gauges installed on either side of the box structure walls. The largest strains, as expected, were measured on the flexible structure and the smallest on the stiff structure. The corner strain gauges (SG8) measured the largest dynamic strains, which are compared with numerical predictions for different structures and motions in Fig. 14 in terms of time histories and Fourier Amplitude Spectra, respectively. Similar to seismic racking and earth pressures, the peak values of dynamic strain were often measured near the effective fundamental frequency of the site (f_{so}'), regardless of the structure"s stiffness. Class-C predictions (default PDMY02) often overestimated bending strains at higher frequencies and underestimated strains at lower frequencies. But the Class-C1 simulations (both mean and upper Darendeli) better captured dynamic strains both in terms of amplitude and frequency content. Similar trends were observed at other locations.

4.5. Summary of numerical and experimental comparisons

The accuracy of Class-C and C1 numerical predictions was evaluated in terms of residuals for different response parameters of interest:

$$\text{Residual } X = \log\left(\frac{X_{\text{experimental}}}{X_{\text{numerical}}}\right) \quad (1)$$

where X refers to a given quantity obtained numerically or experimentally. The variance in the predicted response was also evaluated among different numerical simulations for different motions considered. Fig. 15 summarizes the range of residuals and variances in different response parameters of interest: PGA profile in the far-field and along the structure, acceleration response spectra and Arias Intensity time histories in the far-field surface, racking of the far-field soil and structure, magnitude and location of dynamic thrust time histories, and dynamic bending strain time histories along the structure walls for each type of simulation. In general, Class-C1 predictions with the upper G/G_{max} Darendeli curve provided improved predictions of most response parameters

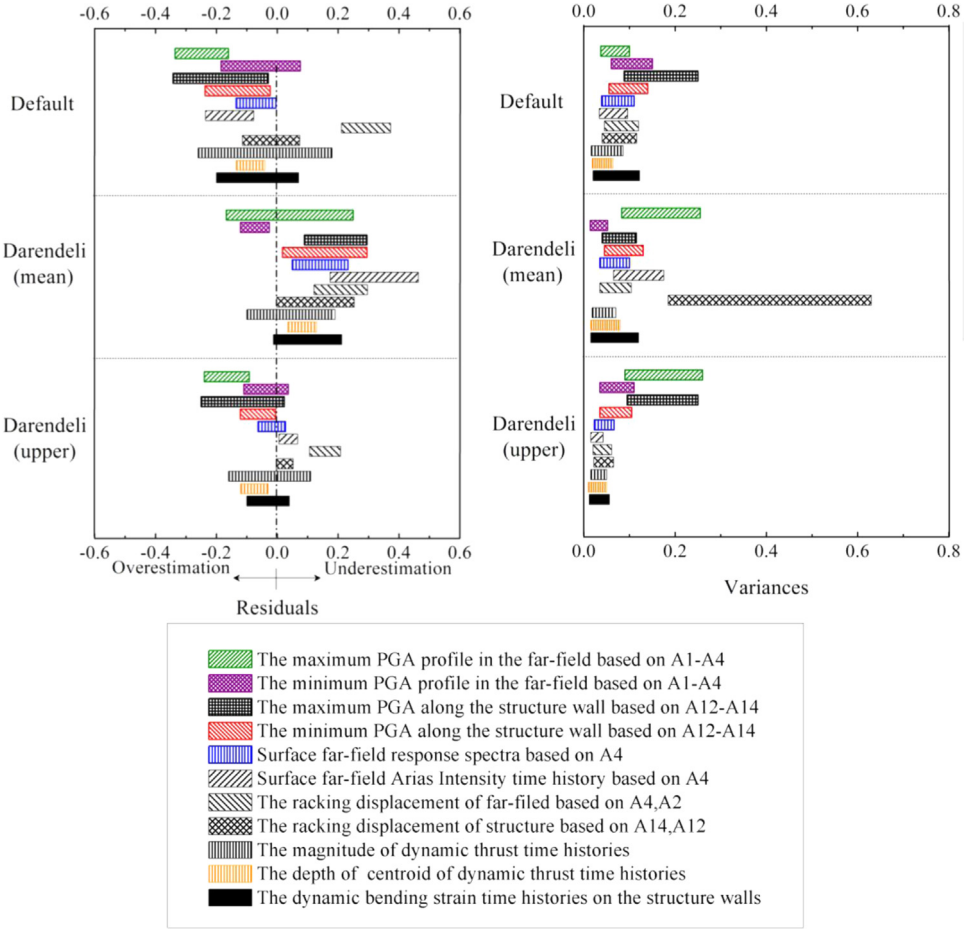

Fig. 15. Range of residuals and variances in the prediction of different response parameters using different simulations.

of interest with a reasonable range of variance. Hence, even though this model was not ideal for all response parameters, overall it captured the seismic demand on and the performance of *stiff-unyielding* underground structures with residuals ranging from about −0.25 to 0.2 and variances of less than approximately 0.3.

5. Concluding remarks

The seismic response of relatively stiff underground reservoir structures that are restrained against rotation at their base and roof is currently not adequately understood. Seismic soil-structure interaction (SSI), structure stiffness, connection to the backfill soil, and soil nonlinearity need to be considered in their design under strong levels of shaking.

A series of Class-C and C1, nonlinear numerical simulations were performed, and their results were compared against centrifuge measurements in terms of site response in the far-field, racking deformation of the soil and structure, and seismic lateral earth pressures and bending strains along the walls of box structures with varying stiffness. Two dimensional (2-D), Class-C, numerical simulations were performed in the finite element program OpenSees with the PDMY02 model. The model parameters were calibrated to capture the response of Nevada sand (test soil) in cyclic simple shear tests. The reduction of soil shear modulus at larger strains (G/G_{max} versus γ) in these simulations was predicted automatically by the nonlinear constitutive model. Class-C1 simulations were subsequently performed with the same constitutive model parameters but with the addition of user-defined G/G_{max} curves proposed by Darendeli [7], which were corrected for soil's implied shear strength. A softer soil response was desired in Class-C1 simulations to improve the predicted accelerations and the overall performance of buried structures. Mean and one standard deviation above mean (upper) G/G_{max} curves proposed by Darendeli [7] for sand were considered in Class-C1 predictions.

The addition of user-defined G/G_{max} curves that were softer than the default PDMY02 model improved the prediction of site response in terms of accelerations and the effective fundamental frequency of the site, but increased the error in far-field settlement predictions. Class-C1 simulations with the upper Darendeli G/G_{max} curve generally led to improved predictions of racking displacements both in the far-field and on the structure. Both sets of Class-C1 simulations also improved the amplitude and frequency content of dynamic earth pressures and thrust. But, all simulations failed to predict the parabolic distribution of dynamic earth pressures on the stiff structure. Class-C1 simulations with the upper Darendeli G/G_{max} curve generally led to better predictions of dynamic bending strains on the structure, both in terms of amplitude and frequency content. The peak response of the structure in terms of racking, bending strains, and seismic earth pressures was shown experimentally to occur near the effective fundamental frequency of the site (f_{so}') regardless of the stiffness of the structure. Class-C1 predictions with the upper Darendeli G/G_{max} curve often predicted this important influence from the dynamic properties of the backfill soil.

In summary, the PDMY02 soil constitutive model with its default shear modulus reduction led to a soil response that was too stiff. This led to the overestimation of f_{so}' as well as the forces and deformations experienced by the buried structure at higher frequencies. The implementation of user-defined, upper Darendeli G/G_{max} curve in OpenSees with the PDMY02 soil constitutive model could better capture the key response parameters of interest both in the far-field and near buried reservoir structures, with residuals ranging from about −0.25 to 0.2 and a variance less than about 0.3. It is acknowledged, however, that the PDMY02 model with many parameters may not always be a practical option. Hence, a comparison of its performance with simpler soil constitutive models in the future will be of value to practitioners.

Acknowledgments

The authors would like to acknowledge the Los Angeles Department of Water and Power (LADWP) for financial support of the experimental component of this research and Mr. Zana Karimi for assistance in developing the OpenSees models of the centrifuge experiments.

References

[1] Al Atik L, Sitar N. Seismic earth pressures on cantilever retaining structures. J Geotech Geoenviron Eng 2010;136(10):1324–33.
[2] Anderson DG, Martin GR, Lam IP, Wang JN. Seismic design and analysis of retaining walls, buried structures, slopes and embankments.Washington, D.C.: Transportation Research Board, National Cooperative Highway Research Program; 2008.
[3] Arulmoli K, Muraleetharan KK, Hossain MM, Fruth LS. VELACS: Verification of liquefaction analyses by centrifuge studies, laboratory testing program.Irvine, CA: The Earth Technology; 1992.
[4] Bardet JP, Huang Q, Chi SW. Numerical prediction for model no. 1. In: Proceedings of the international conference on the verification of numerical procedures for the analysis of soil liquefaction problems. Balkema, Netherlands, vol. 1; 1993. pp. 67–86.
[5] Bolton MD, Steedman RS. Centrifugal testing of micro-concrete retaining walls subject to base shaking. In: Proceedings of conference on soil dynamics and earthquake engineering, southampton. Balkema, Rotterdam. pp. 311–329.
[6] Cilingir U, Madabhushi SG. Effect of depth on the seismic response of square tunnels. Soils Found 2011;51(3):449–57.
[7] Darendeli MB. Development of a new family of normalized modulus reduction and material damping curves.Austin, TX: University of Texas at Austin; 2001.
[8] Dewoolkar MM, Ko H, Pak RYS. Seismic behavior of cantilever retaining walls with liquefiable backfills. J Geotech Geoenviron Eng ASCE 2001;127(5):424–35.
[9] Elgamal A, Yang Z, Parra E. Computational modeling of cyclic mobility and post-liquefaction site response. Soil Dyn Earthq Eng 2002;22(4):259–71.
[10] Gillis K, Dashti S, Hashash Y. Dynamic calibration of tactile sensors for measurement of soil pressures in centrifuge. ASTM Geotech Test J 2015;38:261–74.
[11] Hashash Y, Dashti S, Romero Arduz MI, Ghayoomi M, Musgrove M. Evaluation of 1-D seismic site response modeling of sand using centrifuge experiments. Soil Dyn Earthq Eng J 2015;78:19–31.
[12] Hushmand A, Dashti S, Davis C, Hushmand B, Zhang M, McCartney J, Lee Y, Hu J. Seismic performance of underground reservoir structures: insight from centrifuge modeling on the influence of structure stiffness. J Geotech Geoenviron Eng 2016. http://dx.doi.org/10.1061/GT.1943-5606.0001477 ASCE.
[13] Kammerer A, Wu J, Pestana J, Riemer M, Seed R. Cyclic simple shear testing of Nevada sand for PEER Center, project 2051999.Berkeley, CA: University of California; 2000.
[14] Karimi Z, Dashti S. Seismic performance of structures on liquefiable soils: insight from numerical simulations and centrifuge experiments. J Geotech Geoenviron Eng ASCE 2016. http://dx.doi.org/10.1061/GT.1943-5606.0001479.
[15] Karimi Z, Dashti S. Numerical and centrifuge modeling of seismic soil-foundation-structure-interaction on liquefiable ground. J Geotech Geoenviron Eng ASCE 2015;04015061(14):1–14.
[16] Lambe TW. Predictions in soil engineering. Geotechnique 1973;23(2):149–202.
[17] McGann CR, Arduino P, Mackenzie-Helnwein P. Stabilized single-point 4-node quadrilateral element for dynamic analysis of fluid saturated porous media. Acta Geotech 2012;7(4):297–311.
[18] Mikola R. Seismic earth pressures on retaining structures and basement walls in cohesionless soils.Berkeley, CA: University of California; 2012.
[19] Mononobe N, Matsuo M. On the determination of earth pressures during earthquakes, Proceedings of the World Engineering Congress, vol. 9; 1929. pp. 179–187.
[20] Nakamura S. Reexamination of Mononobe-Okabe theory of gravity retaining walls using centrifuge model tests. Soils Found 2006;46(2):135–46.
[21] Okabe S. General theory of earth pressure. J Jpn Soc Civil Eng 1926;12.
[22] Ortiz LA, Scott RF, Lee J. Dynamic centrifuge testing of a cantilever retaining wall. Earthq Eng Struct Dyn 1983;11(2):251–68.
[23] Psarropoulos PN, Klonaris G, Gazetas G. Seismic earth pressures on rigid and flexible retaining walls. Int J Soil Dyn Earthq Eng 2005;25:795–809.
[24] Roth WH, Mehrain M. The meaning of seismic earth pressure. Annual SEAOC Convention; 2010.
[25] Seed HB, Whitman RV. Design of earth retaining structures for dynamic loads. ASCE specialty conference, lateral stresses in the ground and design of earth retaining structures. Cornell University, Ithaca, New York; 1970. pp. 103–147.
[26] Seed HB, Idriss IM. Soil moduli and damping factors for dynamic response

analyses. Berkeley, CA: Earthquake Engineering Research Center, University of California; 1970. p. 40.
[27] Stadler AT. Dynamic centrifuge testing of cantilever retaining walls.Boulder, Colorado: University of Colorado at Boulder; 1996.
[28] Steedman RS, Zeng X. Centrifuge modeling of the effects of earthquakes on free cantilever walls. *Centrifuge*'91; 1991.
[29] Tessari A, Abdoun T, Sasanakul I, Wroe E. Boundary corrected calibration of tactile pressure sensors. Phys Model Geotech 2014:331–6.
[30] Tsinidis G, Pitilakis K, Madabhushi G, Heron C. Dynamic response of flexible square tunnels: centrifuge testing and validation of existing design methodologies. Geo-technique 2015;65(5):401–17.
[31] Veletsos AS, Younan AH. Dynamic modeling and response of soil-wall systems. J Geotech Eng ASCE 1994;120(12):2155–79.
[32] Wood JH. Earthquake induced soil pressures on structures.Pasadena, CA: California Institute of Technology; 1973.
[33] Wriggers P, Vu VT, Stein E. Finite-element formulation of large deformation impact–contact problems with friction. Comput Struct 1990;37:319–31.
[34] Yang Z, Elgamal A, Parra E. Computational model for cyclic mobility and associated shear deformation. J Geotech Geoenviron Eng 2003;129(12):1119–27.
[35] Yang Z, Lu J, Elgamal A. OpenSees soil models and solid-fluid fully coupled elements: user"s manual.San Diego: Department of Structural Engineering, University of California; 2008.
[36] Zhai E, Davis CA, Yan L, Hu J. Numerical simulations of geotechnical centrifuge Modeling of seismic earth pressures on an underground restrained structure. International Efforts in Lifeline Earthquake Engineering. ASCE; December 2013. pp. 369–376.